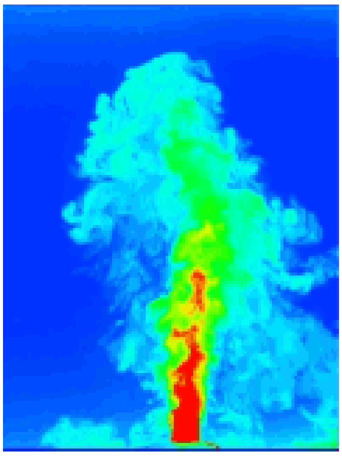

Journal of Turbulence
Publication details, including instructions for authors and subscription information:
http://www.informaworld.com/smpp/title~content=t713665472

Eulerian and Lagrangian statistics in stably stratified turbulent channel flows

Kyongmin Yeo [ab]; Byung-Gu Kim [a]; Changhoon Lee [a]
[a] Department of Mechanical Engineering, Yonsei University, Seoul, Korea [b] Division of Applied Mathematics, Brown University, Providence, RI, USA

First Published on: 01 January 2009

To cite this Article Yeo, Kyongmin, Kim, Byung-Gu and Lee, Changhoon(2009)'Eulerian and Lagrangian statistics in stably stratified turbulent channel flows',Journal of Turbulence, Volume 10, Art. No. N17,

To link to this Article: DOI: 10.1080/14685240902902365

URL: http://dx.doi.org/10.1080/14685240902902365

Journal of Turbulence
Vol. 10, No. 17, 2009, 1–26

Taylor & Francis
Taylor & Francis Group

Eulerian and Lagrangian statistics in stably stratified turbulent channel flows

Kyongmin Yeo[a,b], Byung-Gu Kim[a] and Changhoon Lee[a*]

[a] *Department of Mechanical Engineering, Yonsei University, Seoul 120-749, Korea;* [b] *Division of Applied Mathematics, Brown University, Providence, RI 02912, USA*

(*Received 22 March 2008; final version received 24 January 2009*)

Using direct numerical simulation, we investigate the Eulerian and Lagrangian characteristics of the near-wall turbulence under stable stratification. In the near-wall region, large-scale motions are suppressed by stable stratification, while small-scale motions are enhanced, which leads to the increase of intermittency. It is shown that the modification of the Reynolds shear stress is caused by the increased intermittency and anisotropy. Investigation of acceleration and vorticity reveals that the length scales and timescales of the near-wall coherent vortices are reduced by stratification. The role of baroclinic torque around the near-wall turbulent structures is also discussed. The Lagrangian statistics indicate that the scaled dispersion in the streamwise direction remains unchanged, while those in the spanwise as well as in the wall-normal direction are suppressed by stratification.

Keywords: stable stratification; turbulent channel flow; Lagrangian statistics; direct numerical simulation

1. Introduction

Turbulence subject to stable stratification has been of great interest due to its dynamical significance in the atmospheric sciences and oceanography. This has naturally led to a huge volume of research on this subject, most of which, however, was on the flow not influenced by the solid surface. Even in some literatures that considered near-wall stratified turbulence, the effect of stratification onto the near-wall turbulence was regarded negligibly small. As we will show in our detailed investigation of various Eulerian and Lagrangian characteristics, the near-wall turbulence is quite dramatically modified by stratification.

For homogeneous turbulence, extensive experimental and numerical studies have been performed to investigate the dynamics of turbulence under stable stratification [1–5]. Mètais and Herring [6] performed direct numerical simulations (DNSs) of stably stratified homogeneous turbulence. They argued that the stably stratified flows exhibit a much smaller energy transfer to smaller scales than the unstratified flows and that the reduced energy transfer results in the decrease of the vortex energy at small scales. Kimura and Herring [7] showed in their direct numerical simulation (DNS) of homogeneous turbulence that the vortex structures in strongly stratified turbulence resemble scattered pancakes which are observed in the two-dimensional turbulence. However, they argued that the characteristics

*Corresponding author. Email: clee@yonsei.ac.kr

ISSN: 1468-5248 online only

DOI: 10.1080/14685240902902365
http://www.informaworld.com

of strongly stratified turbulence are different from the two-dimensional turbulence in that energy dissipation at small scales is dominated by horizontal vorticity, a component absent in two-dimensional dynamics. Thoroddsen and van Atta [8] showed that the baroclinically generated vorticity by an axisymmetric vortex has a sign opposite to that of the original point vortex and strongly depends on the azimuthal angle. Diamessis and Nomura [4] found that baroclinic torque acts as a sink which promotes decay of enstrophy in homogeneous sheared turbulence. They also suggested that the local density gradient attenuates vertical vorticity, while shear and baroclinic torque tend to maintain horizontal vorticity, which leads to the development of the pancake-type vortices.

In a turbulent boundary layer, owing to the presence of the wall, turbulent fields become inhomogeneous, which in turn assures that the effects of buoyancy on turbulent quantities will also be dependent on the the distance from the wall. Coleman et al. [9] showed in their DNS of turbulent Ekman layers that the greatest difference between the neutral and stratified flows occurs in the outer region. They found that the stratification reduces the turbulent intensity and motions in the vertical direction and thereby the vertical transport of momentum, which in turn diminishes the rate of turbulent energy production. Garg et al. [10] performed both DNSs and large-eddy simulations (LESs) of stably stratified turbulent channel flows. They showed that the turbulent characteristics of the outer region are different from those in the homogeneous turbulence. Armenio and Sarkar [11] performed LES of turbulent channel flows and showed that the fluctuating motion becomes more horizontal in the outer region like the homogeneous turbulence, while the turbulent structures in the near-wall region are not changed noticeably. Iida et al. [12] showed that the stable stratification selectively modifies turbulent scales: the energy spectra at low wavenumbers are attenuated, while those at high wavenumbers increase by a little.

Literature survey reveals that the modification of turbulent structures in the homogeneous turbulence and in the outer region of a turbulent boundary layer flow is relatively well understood. However, there are only a few results on the turbulent structures in the inner layer, where most important turbulent events such as bursting, production, and dissipation occur. This was due to the fact that investigation of typical turbulence statistics such as turbulence intensities usually reveals that these quantities are not modified as prominently as those in the region far away from the wall. Away from the wall at which local shear intensity is weak, the dynamics are mostly driven by the internal gravity wave. In the near-wall region, however, strong shear intensity makes turbulence field more intermittent [13, 14], which results in a very complicated interaction between a strong shear and density stratification. Therefore, for a more accurate investigation of turbulence modification near the wall by stratification, statistics of vorticity or acceleration which has been known to be directly related with the near-wall intermittent turbulent structures should be considered. [15] Furthermore, no result on the Lagrangian nature of stably stratified turbulence in a boundary layer flow, which is essential in understanding the transport mechanism, has been reported. In this study, we aim to investigate the modification of near-wall turbulent characteristics and of the Lagrangian nature under stable stratification. For our goals, we performed DNS of stably stratified turbulent channel flows, and we present various Eulerian and Lagrangian statistics with a particular emphasis on the near-wall region, which have not been investigated in detail until now. The relevant modification of the near-wall coherent structures by stratification is also discussed.

This paper is organized as follows: numerical methods and computation cases are briefly described in Section 2; Eulerian statistics are presented in Section 3; modification of the near-wall coherent vortices is discussed in Section 4; turbulent scales are examined in Section 5; the Lagrangian statistics are analyzed in Section 6; finally, conclusions are provided.

2. Numerical approach

The continuity, Navier–Stokes, and heat transport equations under the Boussinesq approximation are, in tensor notation,

$$\frac{\partial U_i}{\partial x_i} = 0, \tag{1}$$

$$\frac{\partial U_i}{\partial t} + U_j \frac{\partial U_i}{\partial x_j} = -\frac{\partial p}{\partial x_i} + \frac{1}{Re_\tau} \frac{\partial^2 U_i}{\partial x_j \partial x_j} + Ri_\tau \theta \delta_{i2}, \tag{2}$$

$$\frac{\partial T}{\partial t} + U_j \frac{\partial T}{\partial x_j} = \frac{1}{Pr Re_\tau} \frac{\partial^2 T}{\partial x_j \partial x_j}, \tag{3}$$

in which $x_1,\ x_2,\ x_3$ or x, y, z denote the streamwise, wall-normal, and spanwise coordinates, respectively; U_i denotes the corresponding velocity components and can be decomposed into the mean and fluctuation, i.e. $U_i = \langle U_i \rangle + u_i$; p is pressure; θ is fluctuating temperature and T is total temperature, i.e. sum of mean and fluctuating temperature. The relevant nondimensional parameters, Reynolds, Prandtl and Richardson numbers are, respectively,

$$Re_\tau = \frac{u_\tau \delta}{\nu}, \quad Pr = \frac{\nu}{\alpha}, \quad Ri_\tau = \frac{\beta \Delta T \delta g}{u_\tau^2},$$

where u_τ is the wall-shear velocity; ν is the kinematic viscosity; α is the thermal diffusivity; β is the thermal expansion coefficient; and g is the gravitational acceleration. All variables are nondimensionalized by the channel half-gap δ, the temperature difference between the top and bottom walls ΔT, and u_τ.

The governing equations were numerically solved by using a spectral method: dealiased Fourier and Chebyshev expansions in the horizontal and wall-normal directions, respectively. The time advancement was carried out by employing the Crank–Nicolson scheme for viscous terms and a third-order three-step Runge–Kutta scheme for the nonlinear terms including the buoyancy source term. The pressure gradient was kept constant with the total mass flux being freely changed in all simulations so that the near-wall turbulence level was maintained. The constant wall-temperature condition was used for the thermal boundary condition. Periodic conditions were imposed in the horizontal directions. Simulation parameters are listed in Table 1. Simulations for four different Ri_τ are performed: $Ri_\tau = 0,\ 50,\ 90$, and 120.

Table 1. Simulation parameters: L_x, L_y, and L_z denote the computational domain sizes in x, y, and z directions, respectively; N_x, N_y, and N_z are the number of grid points in the corresponding direction.

Re_τ	Pr	L_x	L_y	L_z	N_x	N_y	N_z
180	0.71	$4\pi\delta$	2δ	$4\pi\delta/3$	128	129	128

The Lagrangian statistics were evaluated by the particle-tracking scheme of Choi et al. [16]. The fluid velocity at the location of a particle was calculated by employing the four-point Hermite interpolation method in the horizontal directions and the Chebyshev interpolation method in the vertical direction. In [16], it was shown that this interpolation method is adequate in the accurate evaluation of the Lagrangian quantities such as acceleration at reasonable computational cost.

3. Eulerian statistics

Arya [17] found in his experiment on the stably stratified boundary layer flows that both the skin friction and the heat transfer rate decrease as the stratification becomes stronger. Figure 1 displays the skin friction coefficient (C_f) and the Nusselt number (Nu) normalized by their counterparts without stratification (C_{f0}, Nu_0) in terms of the Richardson number based on the bulk velocity (U_b); C_f and Nu are defined as

$$C_f = \frac{2\tau_w}{\rho U_b^2}, \tag{4}$$

$$Nu = \frac{2\delta q_w}{kT_b}, \tag{5}$$

in which τ_w is the mean shear stress at the wall; ρ is the density of fluid; T_b is the bulk mean temperature; q_w is the mean heat flux at the wall; and k is the thermal conductivity. The results are compared to the experimental data by Fukui et al. [18] and the numerical

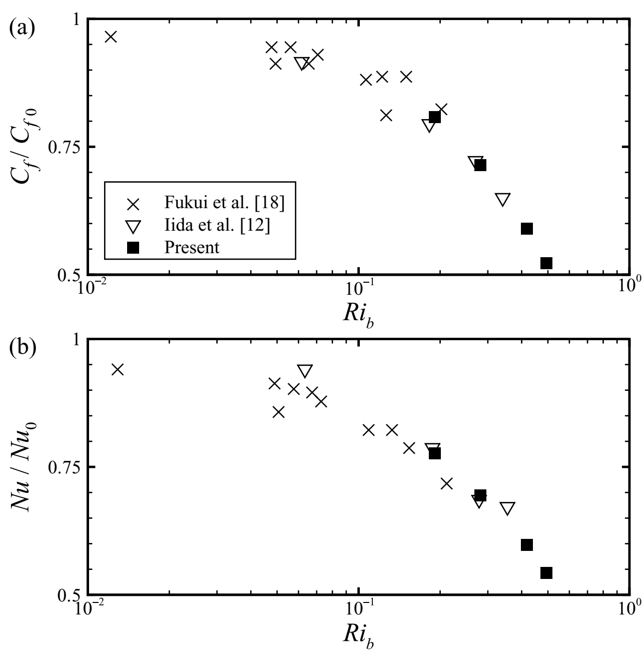

Figure 1. The normalized (a) skin friction coefficient and (b) Nusselt number in terms of the bulk Richardson number.

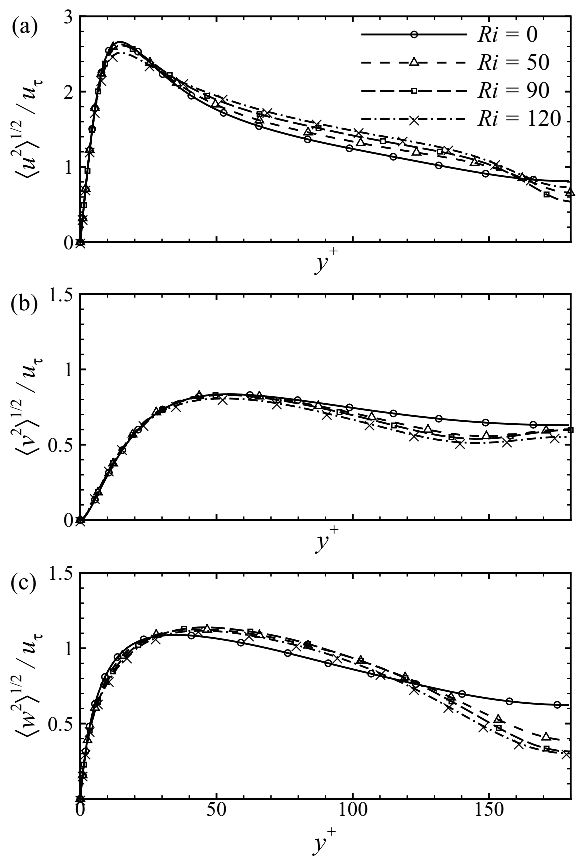

Figure 2. Turbulent intensities normalized by u_τ: (a) streamwise, (b) vertical, and (c) spanwise turbulent intensities.

results by Iida et al. [12]. It is shown that the present results are in good agreement with the previously reported values. With increasing Ri_b, both the normalized skin friction coefficient and the Nusselt number decrease. Since the wall shear is kept constant in our simulation, the decrease of C_f is due to the increased bulk velocity [11].

The turbulent intensities normalized by u_τ are presented in Figure 2, showing that the turbulent intensities are hardly changed by stratification. In the buffer layer ($5 \leq y^+ \leq 30$), the streamwise and spanwise intensities are attenuated a little, while the wall-normal component shows no discernible change. This kind of minor modification of turbulence intensities near the wall has led most previous researchers not to pay attention to the near-wall modification due to stratification. However, as will be shown below and in the following sections, the near-wall modification is far from being of negligible importance. In the region $y^+ \geq 30$, it is observed that the turbulent intensities in the streamwise and spanwise directions are slightly modified, while the change of vertical component is limited to the region away from the wall, $y^+ \geq 80$. The increases of streamwise and spanwise intensities are caused by the steepened velocity gradient which enhances the turbulent production ($\equiv \langle uv \rangle d\langle U \rangle / dy$) in this region [12]. Near the channel center ($160 \leq y^+ \leq 180$), both the

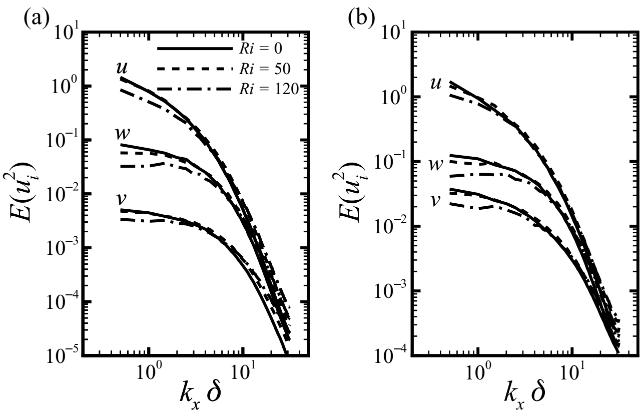

Figure 3. One-dimensional energy spectra obtained at (a) $y^+ \simeq 7$ and (b) $y^+ \simeq 20$.

streamwise and spanwise intensities are decreased rapidly, since turbulent kinetic energy in this region is largely suppressed by the buoyancy dissipation [10].

Figure 3 shows the streamwise energy spectra obtained in the viscous sublayer and buffer layer. It is observed that the turbulent scales are selectively modified, as reported in [12]. The energy in large-scale motions is reduced, while small-scale motions become more energetic. In stably stratified homogeneous flows, it is well known that the kinetic energy is suppressed by buoyancy, which eventually causes turbulence to decay. The loss of energy at large scales is partially compensated by the increased energy at high wavenumbers. Therefore intensities are hardly changed at $y^+ = 7$ and $y^+ = 20$ (Figure 2), instead kinetic energy is redistributed between different scales, leading to the modification of length scales.

Figure 4(a) presents the Reynolds shear stress profiles in wall coordinate. It is shown that the Reynolds shear stress is progressively decreased with increasing Richardson number, indicating the relative importance of viscous stress in stably stratified channel flows [11]. The uv-correlation coefficient shown in Figure 4(b) clearly indicates that stratification tends to reduce the correlation between horizontal and vertical motions, and thus, the vertical transport of momentum and the interaction between layers are weakened in stably stratified flows [9, 10]. It is interesting to note that the local peak at $y^+ \simeq 12$ shown at $Ri_\tau = 0$

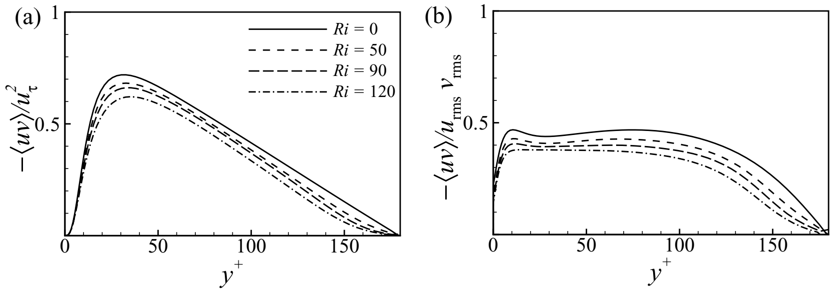

Figure 4. Profiles of (a) the Reynolds stress normalized by u_τ and (b) correlation coefficient of u' and v', in which subscript 'rms' means the r.m.s. value.

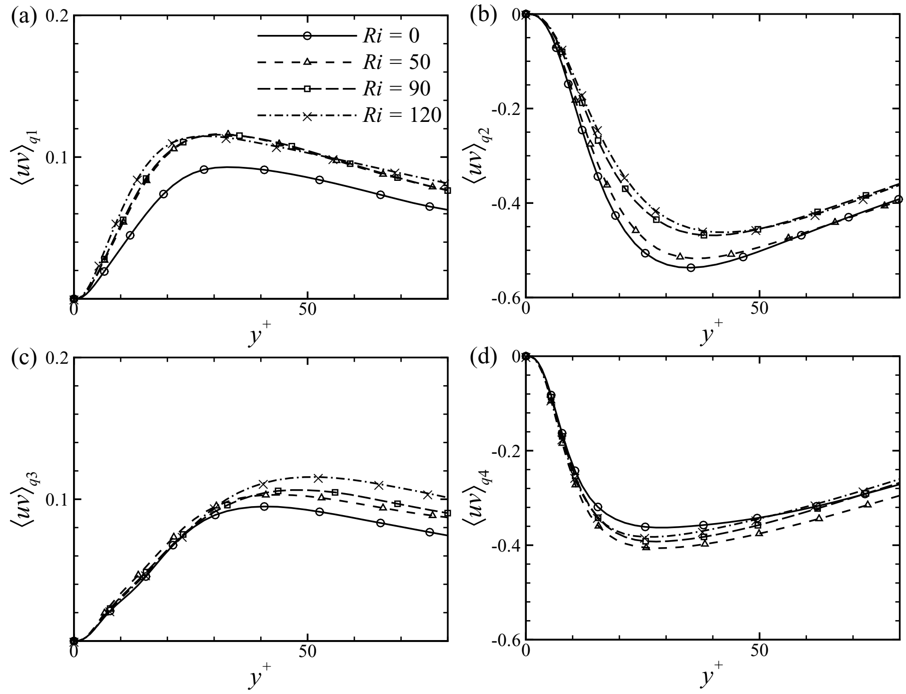

Figure 5. Reynolds stress normalized by u_τ; Reynolds stress from the (a) first, (b) second, (c) third, and (d) fourth quadrants.

case in the correlation distribution is gradually decreased and eventually disappears when $Ri_\tau = 120$. Since the local peak is typically caused by the near-wall coherent structures responsible for the kinetic energy production [19, 20], the mitigation of the peak suggests that the near-wall coherent structures are modified by the stable stratification.

To investigate the modification of the Reynolds shear stress in detail, the quadrant analysis of the Reynolds stress was performed. Figure 5 shows the Reynolds stress from each quadrant event, that is,

$$\langle uv\rangle = \langle uv\rangle_{q1} + \langle uv\rangle_{q2} + \langle uv\rangle_{q3} + \langle uv\rangle_{q4}, \tag{6}$$

in which the sub script 'qi' denotes to which quadrant event the fractional Reynolds stress belongs. The first quadrant, $u > 0,\ v > 0$, implies outward high-speed motion; the second quadrant, $u < 0,\ v > 0$, denotes ejection events; the third quadrant, $u < 0,\ v < 0$, indicates inward low-speed motion; the fourth quadrant, $u > 0,\ v < 0$, contains sweep events. Although the total Reynolds stress monotonously decreases across the channel, the fractional Reynolds stress from each quadrant event shows complex behaviors in the presence of stratification. In the near-wall region ($y^+ \leq 30$), the magnitudes of $\langle uv\rangle_{q1}$ and $\langle uv\rangle_{q4}$ are increased, while $\langle uv\rangle_{q2}$ is attenuated, and $\langle uv\rangle_{q3}$ does not show a significant change. In other words, the magnitude of sweep events is significantly increased, whereas the ejection events are suppressed in the near-wall region. In neutral flows, $\langle uv\rangle_{q2}$ becomes larger than $\langle uv\rangle_{q4}$ when $y^+ \geq 12$ [19]. However, in stratified flows, the crossover point moves away from the wall. $\langle uv\rangle_{q2}$ becomes larger than $\langle uv\rangle_{q4}$ when $y^+ \geq 18,\ 22$, and 24 for $Ri_\tau = 50$, 90, and 120, respectively.

Figure 6(a–d) presents the weighted probability density functions (p.d.f.s) of the Reynolds stress from each quadrant in the buffer layer ($y^+ \simeq 20$). The weighted p.d.f. is defined as

$$H(uv_{qi}) = \mathrm{Pdf}\left(\frac{|uv_{qi}|}{u_{\mathrm{rms}}v_{\mathrm{rms}}}\right)\frac{|uv|}{u_\tau^2}. \tag{7}$$

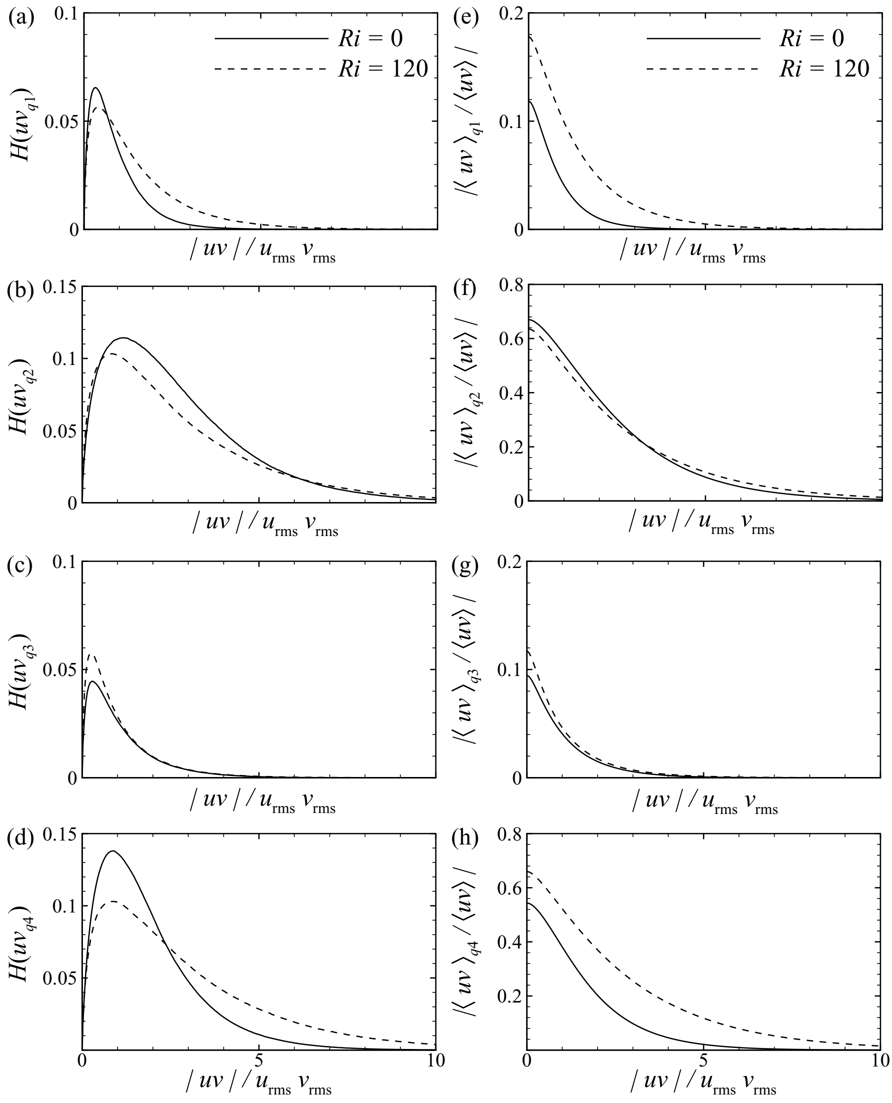

Figure 6. Weighted p.d.f.s of quadrant events and fraction contribution to the Reynolds stress in terms of the Reynolds stress normalized by $\langle u^2\rangle^{1/2}$ and $\langle v^2\rangle^{1/2}$: weighted p.d.f.s of (a) first-, (b) second-, (c) third-, and (d) fourth-quadrant events and fractional contribution to the Reynolds stress from the (e) first, (f) second, (g) third, and (h) fourth quadrants.

It is found that the increased magnitudes of the first- and fourth-quadrant events mainly come from intense-$|uv|$ events; $H(uv_{q1})$ and $H(uv_{q4})$ at $Ri_\tau = 120$ show longer tails compared to the neutral case, indicating that the turbulent field becomes more intermittent; $H(uv_{q1})$ and $H(uv_{q4})$ are decreased when $|uv|/u_{\rm rms}v_{\rm rms}$ is less than about 0.6 and 2.2, respectively; $H(uv_{q2})$ is decreased when $0.7u_{\rm rms}v_{\rm rms} \le |uv| \le 6u_{\rm rms}v_{\rm rms}$, while that of large-magnitude events is not modified significantly. Interestingly, only $H(uv_{q3})$ shows increase at the small-magnitude events, that is, $|uv| \le 1.4u_{\rm rms}v_{\rm rms}$.

The fractional contributions from the four-quadrant events to the Reynolds stress in terms of the threshold of $|uv|/u_{\rm rms}v_{\rm rms}$ at $y^+ \simeq 20$ are illustrated in Figure 6(e–h) [21, 19]. The contribution from the fourth-quadrant events to the Reynolds stress is larger than that of the second-quadrant events, unlike the $Ri_\tau = 0$ case. The contributions from the first- and fourth-quadrant events become larger in the stably stratified flows. The contribution from the second-quadrant events at $Ri_\tau = 120$ becomes larger than that of neutral flow when $|uv|/u_{\rm rms}v_{\rm rms} \ge 3.3$.

Overall, the changes in the Reynolds stress are caused not only by the suppression of the small-$|uv|$ events but also by the increased intense-$|uv|$ events, which is consistent with the selective modification of turbulent scales shown in the energy spectra (Figure 3).

4. Modification of the near-wall coherent vortices

The vorticity fluctuations, which are closely related with the coherent structures, are illustrated in Figure 7. The root-mean-square (r.m.s.) vorticities in the region $y^+ \le 5$ are not modified significantly, whereas beyond the viscous sublayer ($5 \le y^+ \le 150$) the vorticity fluctuations are intensified in all directions as Ri_τ increases. Noticeable increase in vorticities with hardly modified velocities suggests that the length scales are reduced, consistent with our observation of energy spectra. In the channel center region, where the effect of stratification is the strongest, turbulence is noticeably decreased, and the internal gravity waves become dominant structures [11, 12]. Therefore, ω_x and ω_y are suppressed in the center region, while ω_z increases slightly.

La Porta et al. [22] showed that the fluid acceleration is a highly intermittent variable, and Lee et al. [15] found that the main source of the acceleration intermittency are the centripetal accelerations appearing around vortices, suggesting that investigation of the acceleration statistics in the near-wall region might reveal the characteristics of the coherent vortices. Figure 8 presents the wall-normal correlation coefficient of the wall-normal acceleration (a_y) for the reference location $y^+_{\rm ref} \simeq 5$. The definition of the wall-normal correlation coefficient is

$$\rho_{ay}(y^+) = \frac{\langle a_y(y^+)a_y(y^+_{\rm ref})\rangle}{\langle a_y^2(y^+)\rangle^{1/2}\langle a_y^2(y^+_{\rm ref})\rangle^{1/2}}. \tag{8}$$

For $Ri_\tau = 0$, a negative peak appears at $y^+ \simeq 30$ and the correlation becomes zero at $y^+ \simeq 20$. Because of the centripetal nature of acceleration, the negative peak and zero-crossing location respectively indicate the ensemble-averaged diameter and center of the streamwise vortices. In stably stratified flows, it is found that the negative peak and zero-crossing location gradually move toward the wall. Figure 9 shows the two-point correlation of a_z evaluated at $y^+ \simeq 20$. Like the wall-normal correlation of a_y, the two-point correlation of a_z also decays faster with increasing Ri_τ. All of these observations naturally

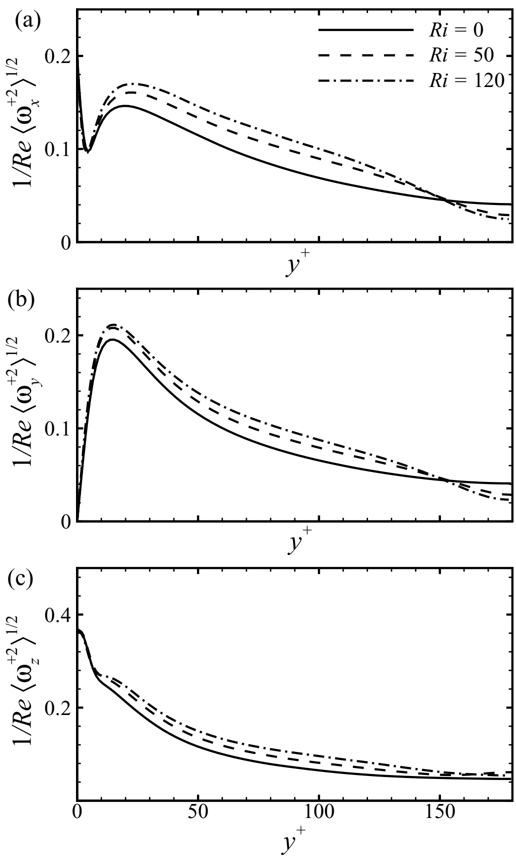

Figure 7. The r.m.s. values of (a) streamwise, (b) wall-normal, and (c) spanwise vorticity fluctuation at three Richardson numbers.

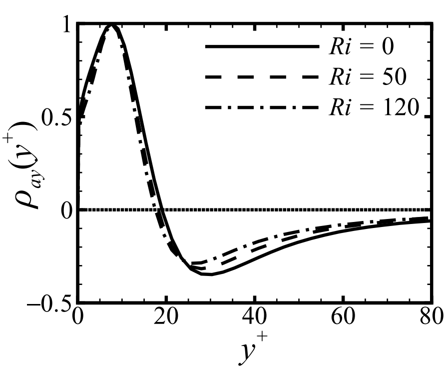

Figure 8. Wall-normal correlation coefficient of wall-normal acceleration for the reference location $y^+ \simeq 5$.

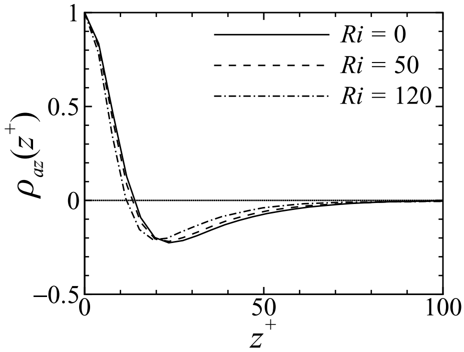

Figure 9. Spanwise correlation coefficient of spanwise acceleration.

lead to the mean diameter of the coherent vortices being reduced by the effect of stable stratification.

Lee et al. [15] showed that the acceleration-magnitude-weighted mean of the cosine of the angle between accelerations of a fluid particle at t_0 and $t_0 + t$ represents the mean time taken for a fluid particle to rotate following the motion of a vortex. In turbulent channel flows, since most vortices in the near-wall region are roughly aligned with the streamwise direction, it is sufficient to evaluate the cosine of angle projected onto the y–z plane to investigate the rotation of acceleration vector. The cosine of angle projected onto the y–z plane is defined as

$$\xi = \cos^{-1}\left(\frac{\tilde{\boldsymbol{a}}(t_0)\cdot\tilde{\boldsymbol{a}}(t_0+t)}{|\,\tilde{\boldsymbol{a}}(t_0)||\tilde{\boldsymbol{a}}(t_0+t)|}\right), \tag{9}$$

$$f(\xi, t) = \frac{\langle |\boldsymbol{a}(t_0)||\boldsymbol{a}(t_0+t)|\cos(\xi)\rangle}{\langle |\boldsymbol{a}(t_0)^2|\rangle^{1/2}\langle |\boldsymbol{a}(t_0+t)^2|\rangle^{1/2}}, \tag{10}$$

in which

$$\tilde{\boldsymbol{a}} = \boldsymbol{a} - (\boldsymbol{a}\cdot\boldsymbol{e}_1)\boldsymbol{e}_1 \tag{11}$$

and $\boldsymbol{e}_i$ is a unit vector in the i direction. Figure 10 shows $f(\xi, t)$ for the fluid particles released at $y^+ \simeq 20$, where the averaged center of the streamwise vortices locates. It is found that the zero-crossing time becomes shorter with increasing stratification, indicating that the time taken for a fluid particle to rotate following the motion of a vortex is shortened. In other words, the angular velocity, or vorticity, of a streamwise vortex becomes larger, which explains the increase of vorticity fluctuations in stably stratified channel flows (Figure 7).

The vorticity equation is given by

$$\frac{D\omega_i}{Dt} = S_{ik}\cdot\omega_k + \frac{1}{Re}\frac{\partial^2\omega_i}{\partial x_k\partial x_k} + Ri_\tau\epsilon_{ij2}\frac{\partial\theta}{\partial x_j}, \tag{12}$$

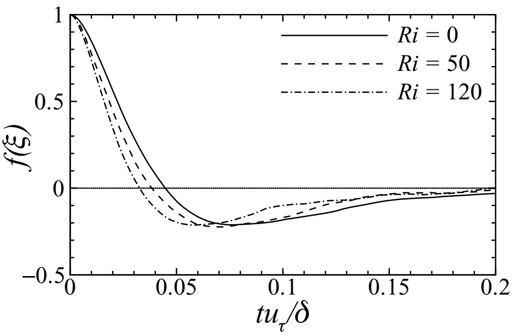

Figure 10. Rotation of acceleration vectors evaluated at $y^+ \simeq 20$.

where S_{ik} is the strain rate tensor. The first, second, and last terms on the right-hand side represent the vortex stretching ST_i, the viscous torque VT_i, and the baroclinic torque Γ_i, respectively. Because the Boussinesq approximation was adopted in this study, the gradient of fluctuating temperature, $\epsilon_{ij2}(\partial\theta/\partial x_j)$ (hereafter referred to as γ_i), represents the baroclinic torque modulo the amplitude Ri_τ, meaning that $\Gamma_i = Ri_\tau \gamma_i$.

Equation 12 clearly suggests that the baroclinic torque affects vorticities in the x and z directions, but it is inactive in the y direction. Therefore it is supposed that the baroclinic torque mainly influences structures aligned in the streamwise and spanwise directions. The p.d.f.s of γ_x and γ_z at particular wall-normal locations are shown in Figure 11. As the intermittency of turbulence increases near the wall [13, 14], the tails of the p.d.f.s become longer even in the neutral case ($Ri_\tau = 0$). In the stably stratified turbulence the kinetic energy in large scales is suppressed, while small scales become more energetic, which contributes to the increase of the intermittency observed in the p.d.f.s of γ_z at $Ri_\tau = 120$ in the region $|\gamma_z| > 3$. This clearly suggests that stratification in the near-wall region, via the baroclinic torque, directly influences the intermittent structures, thus enhancing intermittent nature. The p.d.f.s of γ_x are symmetric, while those of γ_z show remarkable asymmetry. This asymmetry becomes more pronounced as the distance from the wall increases. The reason for this asymmetry is that high-temperature-gradient regions, the so-called microfronts, are created by a collision of two local outflows between legs of a horseshoe vortex, mostly formed in pairs head-up and head-down [23, 24]. It should be noted that the streamwise variation of fluctuation temperature contributes most to the spanwise torque. Even for an asymmetric single-leg horseshoe vortex, the microfront which is composed of strong negative temperature gradient is still caused by the cool fluid impinging on the upper warm fluid. On the other hand, regions of positive, relatively weak temperature gradient are widely spread.

Figure 12(a) shows that in neutral flows, strong positive/negative baroclinic torques are found in the fringe regions of strong negative/positive streamwise vortices. In this neutral, gravity-free flow, γ_x has no effect on the vorticity field. When gravity is turned on, however, γ_x acts as an active source modifying turbulent structures. Then small-size streamwise structures would be generated by the baroclinic torque counter-rotating against existing vortices. Figure 12(c) shows that small-size vortical structures are not only generated but also maintained in a stably stratified flow. Figure 12(b, d) represents total temperature profiles across vortices. When the Richardson number is zero, the sign of γ_x of inner cores is the same as vortices. Therefore, the vortex core would be strengthened during the

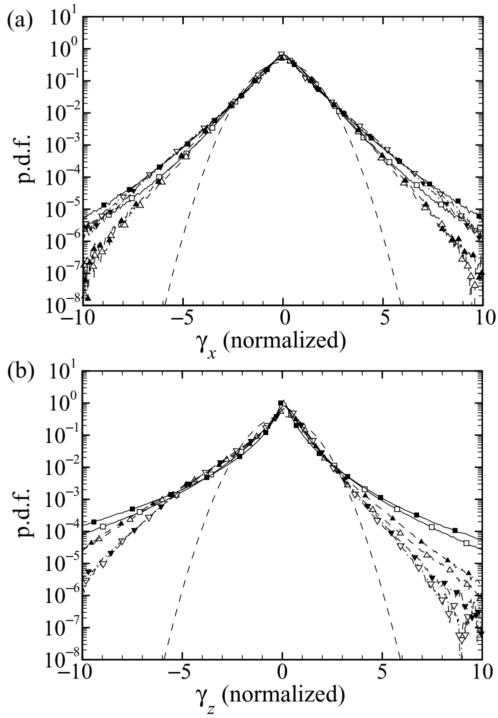

Figure 11. Normalized p.d.f.s of the temperature gradient fluctuation (γ_i) obtained from the lower half of the channel at $Ri_\tau = 0$ and 120: (a) streamwise components γ_x; (b) spanwise components γ_z; □ and ■, $y^+ = 5$; △ and ▲, $y^+ = 20$; ▽ and ▼, $y^+ = 50$; — — —, normal Gaussian. Open and solid symbols denote $Ri = 0$ and 120 respectively.

initial transition of stratification starting from neutral condition. For the $Ri_\tau = 120$ case, however, Figure 12(d) shows that the temperature gradient is opposite in the fringe of a vortex. It would result in increased vorticity. Therefore increased r.m.s. vorticity can be partly explained by this corotating baroclinic torque as well as by reduced length scales.

The p.d.f.s of Γ_x/ST_x, the ratio of the streamwise baroclinic torque to vortex stretching, and Γ_x/VT_x, the ratio of the streamwise baroclinic torque to viscous torque, are shown in Figure 13(a, c). Both p.d.f.s show a peak at zero torque ratio, which means that in most regions baroclinic torques are smaller, albeit nontrivial, than vortex stretching or viscous torque. However, their corresponding magnitude of squared Γ_x shown in Figure 13(b, d) is smallest at zero torque ratio where the p.d.f.s are highest. On the other hand, high magnitudes are found when each torque ratio is high, clearly indicating that most contribution in modifying vortex structures is from less probable events.

Figure 14 shows vortical structures identified by the so-called λ_2 method [25] for the neutral and stratified cases. The legs of a hairpin vortex typically make an angle with the bottom surface in the neutrally stratified flow. Diamessis and Nomura [4] showed that turbulent structures tend to flatten and decline as Ri increases in homogeneous sheared turbulence. Li et al. [26] also found that the angle of hairpin vortices in the buffer layer is decreased in drag-reduced flow by surfactant additive compared with pure water flow. In our flow affected by baroclinic torque, however, the angle of leg measured from the surface is increased compared to that of the neutral flow, whereas the angle of the head decreases.

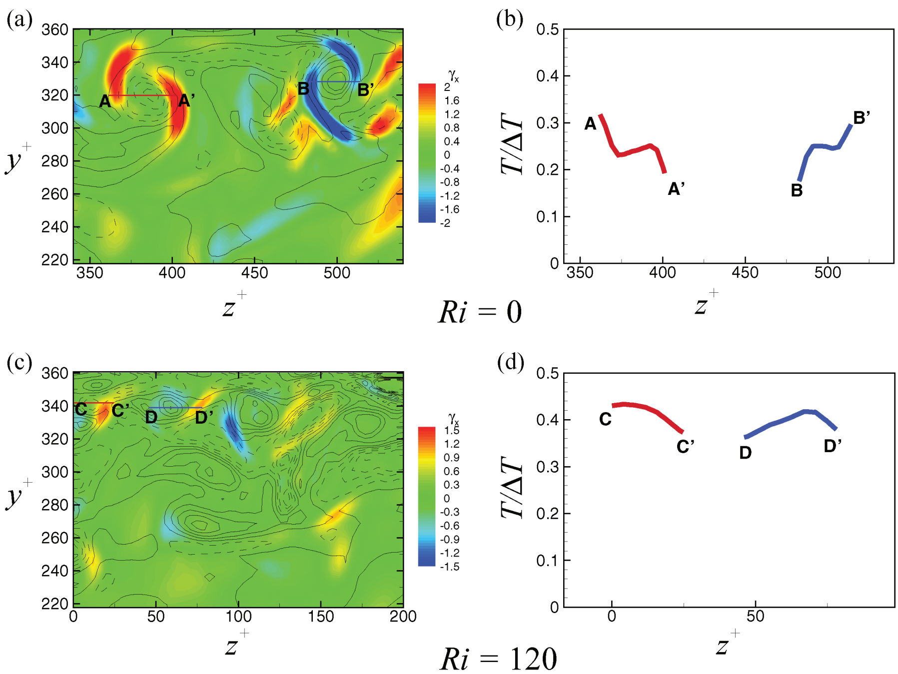

Figure 12. Snapshots of the fluctuating components of the streamwise vorticity ω_x (lines) and the streamwise temperature gradient γ_x (contours) at (a) $Ri_\tau = 0$ and (c) $Ri_\tau = 120$. Solid and dotted lines represent positive and negative vorticity, respectively. Temperature profiles across vortex structures are shown in (b) and (d).

It can be easily seen that a strong negative spanwise baroclinic torque near the head and positive torque above the leg act on the part between the head and the tip of the leg, resulting in the increase of the angle of the leg and the decrease of the angle of the head. By the same action of the negative torque near the head, the head part of a vortex in the stratified flow is found further away from the wall compared to that of the neutral flow.

Zhou et al. [27] indicated that the direction of vorticity vector is not always aligned with the direction of vortical structure. Deviation between a coherent structure and the direction of vorticity inside the structure for neutral flow is demonstrated in Figure 15(a). Figure 15(b) shows that, for $y^+ < 20$, vorticities are highly tilted up compared to the corresponding vortical structures. Despite such inconsistency, it still is worthwhile to investigate the modification of vorticity orientation under stratification. When $y^+ > 20$, however, the direction of vorticity is well aligned with that of vortical structures as shown in the figure.

The polar angle of $\boldsymbol{\omega}'$ measured from x–z plane is estimated from

$$\Phi = cos^{-1}\left(\frac{\boldsymbol{\omega}' \cdot \boldsymbol{\omega}'_p}{|\boldsymbol{\omega}'||\boldsymbol{\omega}'_p|}\right), \tag{13}$$

in which $\boldsymbol{\omega}'_p$ denotes $\boldsymbol{\omega}'$ projected on the wall (Figure 16). In the log-law region, the average angle of vorticities is around 33° under the neutral condition ($Ri_\tau = 0$). Our result agrees well with the recent experimental result that the most frequently observed angle was 38° at $y^+ = 110$ and 33° in the outer wake region [28]. Under stratification, this angle is hardly

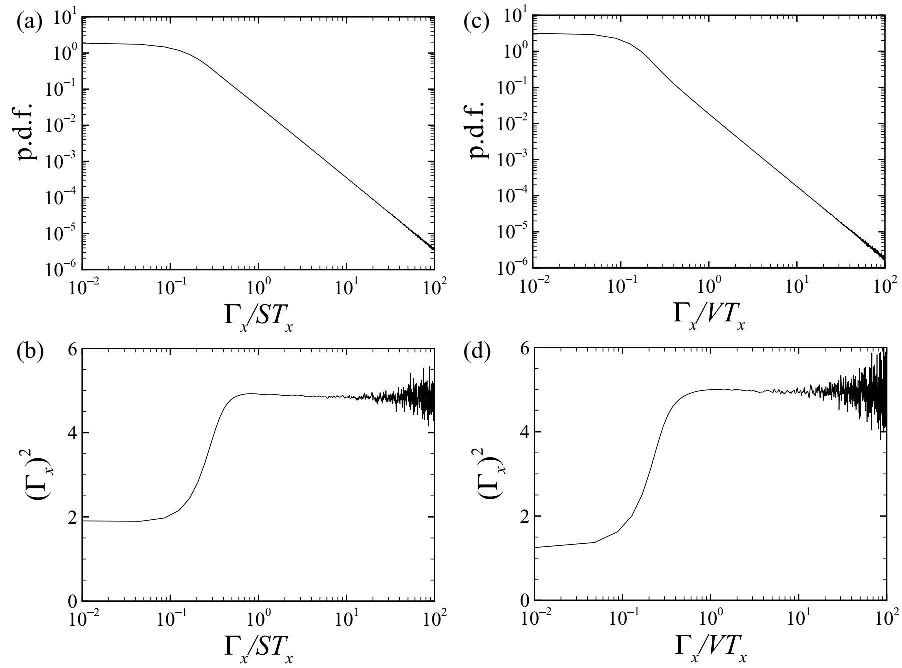

Figure 13. (a) The p.d.f. of the ratio of the streamwise baroclinic torque to the streamwise vortex stretching obtained at $y^+ = 20$ for $Ri = 120$. (b) Corresponding squared baroclinic torque. (c) The p.d.f. of the ratio of the streamwise baroclinic torque to the streamwise viscous torque at $y^+ = 20$ for $Ri = 120$. (d) Corresponding squared baroclinic torque. The left half of each figure is omitted due to the symmetry.

modified near the wall, although there is a drastic change in the channel center region. However, when the angle of vorticity inside the coherent structures is investigated, there is a noticeable change. In the region $y^+ \leq 40$, the angle increases, while in the region $y^+ = 40 \sim 120$, the angle decreases as shown in the comparison of the angle of filtered data. Considering that each region corresponds to the typical region in which the leg and head of horseshoe vortices are found, this observation agrees well with our investigation of vortical structures above (see Figure 14). In the sublayer, a slight increase of the angle can be observed, which does not necessarily mean the corresponding change of the orientation of structures, since this angle does not correctly represent the orientation of the imbedding structure as shown in Figure 14.

5. Length scales and timescales

The averaged dissipation rate of turbulent kinetic energy is defined as

$$\langle \epsilon \rangle = \frac{\nu}{2} \left\langle \left(\frac{\partial u_i}{\partial x_j} + \frac{\partial u_j}{\partial x_i} \right) \left(\frac{\partial u_i}{\partial x_j} + \frac{\partial u_j}{\partial x_i} \right) \right\rangle. \tag{14}$$

In homogeneous turbulence, it is well known that $\langle \epsilon \rangle$ is reduced under stable stratification, which in turn makes the Kolmogorov scales grow [6, 29]. Figure 17 displays $\langle \epsilon \rangle$ profiles

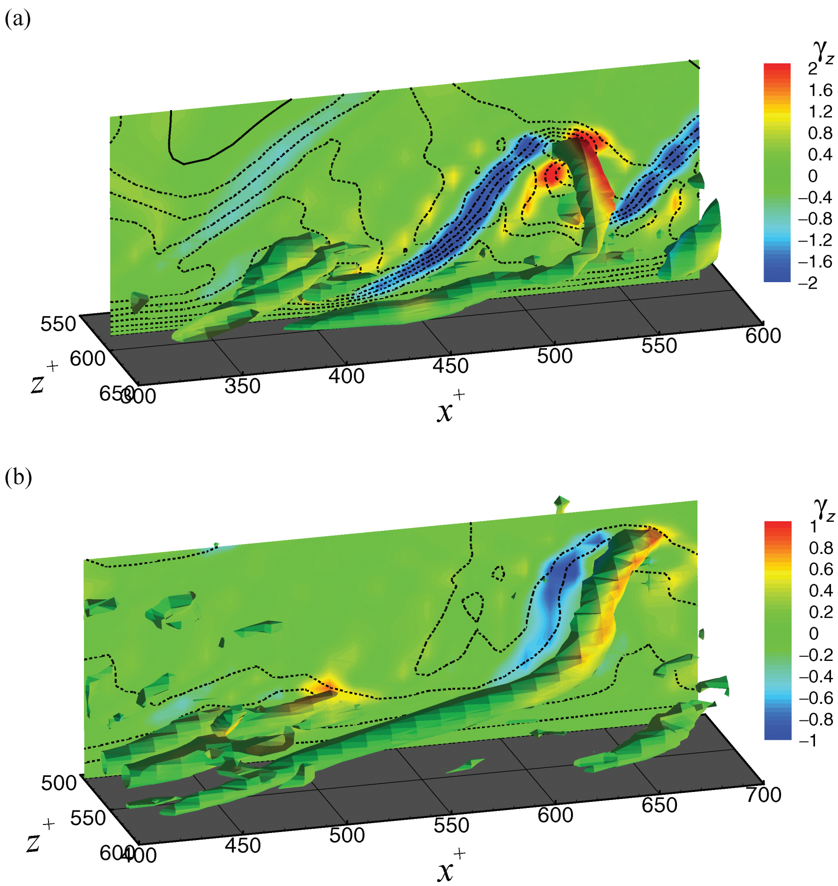

Figure 14. Vortical structures identified by the λ_2 method. Flooding and line contours represent the temperature gradient fluctuation in the spanwise direction, γ_z, and temperature, respectively.

normalized by the wall units, clearly showing that $\langle\epsilon\rangle$ is almost unchanged in the viscous sublayer ($y^+ \leq 5$), while in the region $5 \leq y^+ \leq 160$, $\langle\epsilon\rangle$ increases with Ri_τ. Major difference between the near-wall turbulence and homogenous turbulence is that the near-wall turbulence contains dominant coherent structures mainly aligned in the streamwise direction, which under stable stratification become smaller as shown in the previous section. This decrease in length scale along with almost invariant turbulence intensities increases dissipation. In the channel center region ($160 \leq y^+ \leq 180$), the decrease of $\langle\epsilon\rangle$ is observed, similar to the case of stably stratified homogeneous turbulence.

In stably stratified turbulence, turbulence is modified by the coexistence of the coherent turbulent motions and gravity waves and the interaction between them. An important timescale of the gravity waves is the Brunt–Väisälä frequency N. Figure 18(a) presents the buoyancy timescale N^{-1} normalized by the wall units, which shows that the buoyancy timescale becomes smaller as Ri_τ increases. In other words, the smallest timescale of motion affected by buoyancy becomes smaller as the stratification effect becomes larger. Since the near-wall peak value of the r.m.s. vorticity in the streamwise direction is in the range of $y^+ = 25$–30 [see Figure 9(a)], the buoyancy obviously influences the near-wall structures. Figure 18(b) shows the Kolmogorov timescale normalized by the buoyancy

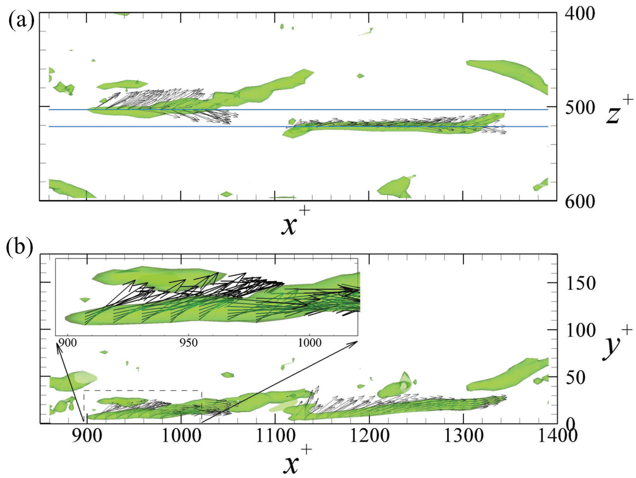

Figure 15. Vortical structures and vorticity vectors for $Ri_\tau = 0$. The vortical structures are identified by isosurfaces of $\lambda_2 = -1500$: (a) $x - z$ plane and (b) $x - y$ plane.

timescale. In the near-wall region, the Kolmogorov timescale is sufficiently smaller than the buoyancy timescale and, thus, there still is a room for small-scale motion which is intact. On the other hand, since the buoyancy timescale becomes of almost the same order as the Kolmogorov timescale in the center region, most turbulent characteristics in the region are conspicuously changed.

In stably stratified flows, it is well known that the buoyancy suppresses large scales of motion. The Ozmidov scale L_O is an estimate of the smallest scale of motion suppressed by the buoyancy; L_O normalized by the Kolmogorov length scale is shown in Figure 19. It is shown that L_O is decreased under stable stratification, indicating that the range of scales available to the turbulence is reduced with the increasing buoyancy effect. In the buffer layer, L_O normalized by wall units is about 70, 60, and 40 for $Ri_\tau = 50, 90,$ and 120, respectively. Considering that the mean diameter of streamwise vortices is about 30 in wall units, L_O is still larger than the size of coherent vortices, and hence the modification of the

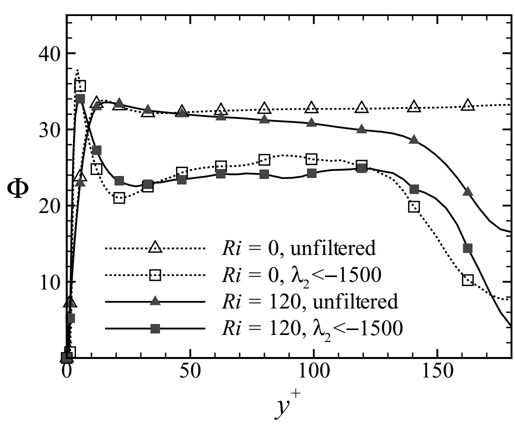

Figure 16. Averaged polar angle of the vorticity vector measured from the $x - z$ plane.

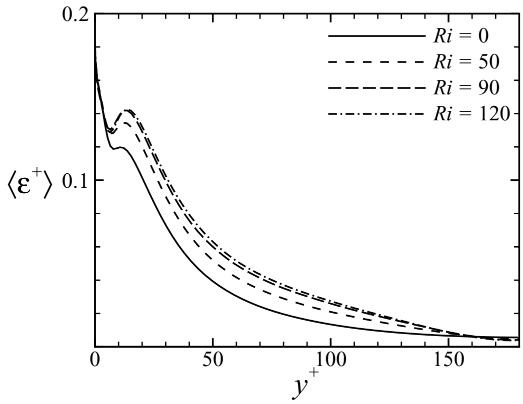

Figure 17. Profiles of the dissipation rate normalized by the wall units.

near-wall coherent vortices by buoyancy is marginal. In the center region, L_O/η is of the order of unity, suggesting that most turbulent motions in the center region are suppressed by buoyancy, and thus the internal gravity waves become a dominant structure in the region.

6. Lagrangian statistics

6.1. *Dispersion statistics*

The study on the Lagrangian nature of turbulence has attracted much interest owing to its applicability to practical use such as the prediction of pollutant dispersion. In this and the following sections, we investigate the Lagrangian nature of stratified near-wall turbulence,

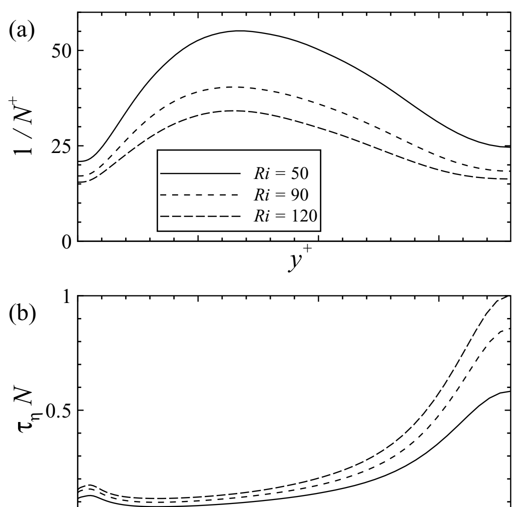

Figure 18. (a) The buoyancy timescale (N^{-1}) normalized by the wall units and (b) the Kolmogorov timescale normalized by the buoyancy timescale.

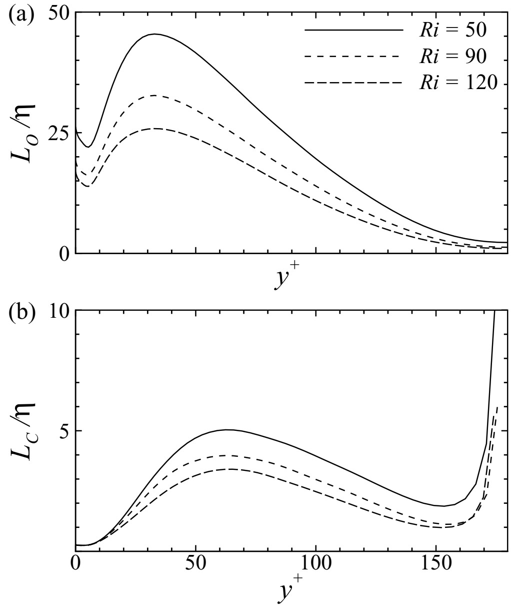

Figure 19. The (a) Ozmidov and (b) Corrsin scales normalized by the Kolmogorov length scale.

with a particular emphasis on dispersion nature. In stably stratified homogeneous turbulence, Csanady [30] theoretically predicted the suppression of dispersion in the direction of stratification. Kimura and Herring [7] confirmed the suppression of dispersion in their DNS of homogeneous turbulence in the presence of stable stratification, although the suppression is much weaker than the previous theoretical predictions [30, 31]. In turbulent channel flows, however, owing to the presence of mean velocity and inhomogeneity caused by the wall, the nature of dispersion will be different from that in homogeneous turbulence. The dispersion in neutral channel flows has been studied by [16], while that in stably stratified channel flows has not been investigated yet.

The mean-square dispersion in i direction is defined as

$$\sigma_{Xi}^2(t) = \left\langle \left(X_i\left(t_0 + t, X_i^0\right) - X_i\left(t_0, X_i^0\right)\right)^2 \right\rangle, \tag{15}$$

in which X_i denotes the location of a fluid particle released at t_0 whose initial position is X_i^0. Applying the classical Taylor's theory to homogeneous flows with uniform mean streamwise velocity U, we obtain scaling relations for σ_X^2,

$$\sigma_{Xi}^2(t) = \left(U^2\delta_{i1} + \left\langle u_i^2\right\rangle\right)t^2, \qquad t \ll T_{Li}, \tag{16}$$

$$\sigma_{Xi}^2(t) = U^2 t^2 \delta_{i1} + 2\left\langle u_i^2\right\rangle T_{Li} t, \quad t \gg T_{Li}, \tag{17}$$

in which T_{Li} is the Lagrangian integral timescale. Scaled dispersion, which is σ_{Xi}^2 normalized by $(U^2\delta_{i1} + \langle u_i^2\rangle)\tau_\eta t$, was obtained for three release locations; each one in the buffer layer, log-law region, and channel center. About 1.3×10^5 sample trajectories were used to evaluate the dispersion from each initial location.

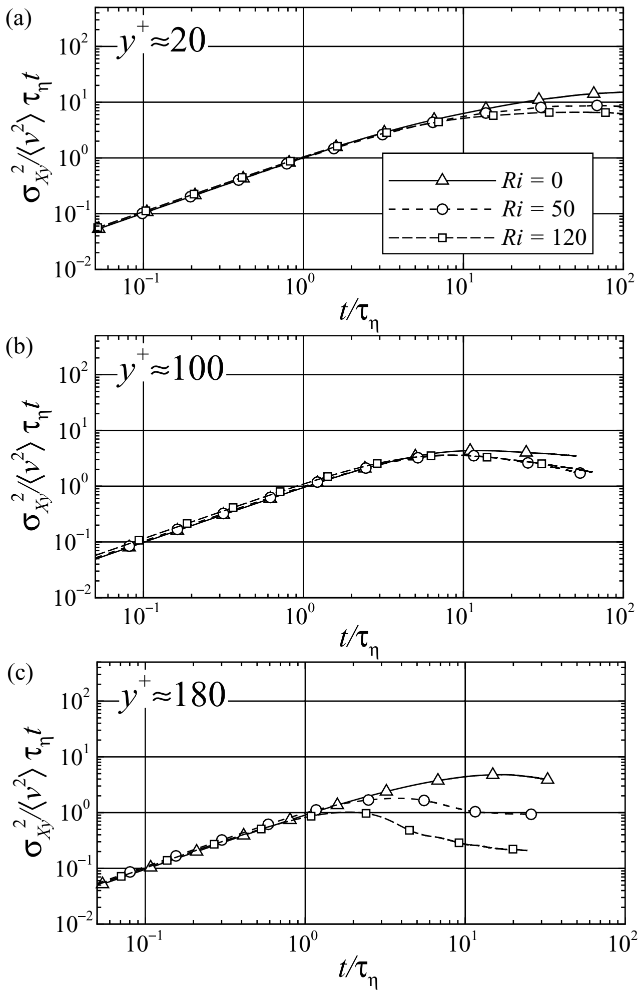

Figure 20. Mean-square dispersion of fluid particles in the wall-normal direction for three different Ri_τ. The fluid particles are released at (a) the buffer layer ($y^+ \simeq 20$), (b) log-law region $y^+ \simeq 100$, and (c) channel center $y^+ \simeq 180$.

The scaled dispersion in the wall-normal direction is shown in Figure 20. The scaled σ_{Xy}^2 is in the initial Taylor range, $\sim t^2$ in early time ($t < \tau_\eta$). It is also confirmed that the scaled σ_{Xy} is 1 at $t/\tau_\eta = 1$. However, just after some τ_η, the scaled σ_{Xy}^2 starts to decrease, indicating that the dispersion in the stratification direction is substantially reduced as shown in the homogeneous flows [7]. Since the large-scale motion is suppressed in stably stratified turbulence, there is less chance for a fluid particle to obtain enough energy to migrate penetrating stable density layers. Consequently the dispersion in the direction perpendicular to the density layers, or the direction of stratification, is reduced. In the channel center region, since the buoyancy timescale is comparable to the Kolmogorov timescale [Figure 18(b)], the scaled σ_{Xy} for $Ri_\tau = 120$ starts deviating from the neutral case just after $1\tau_\eta$.

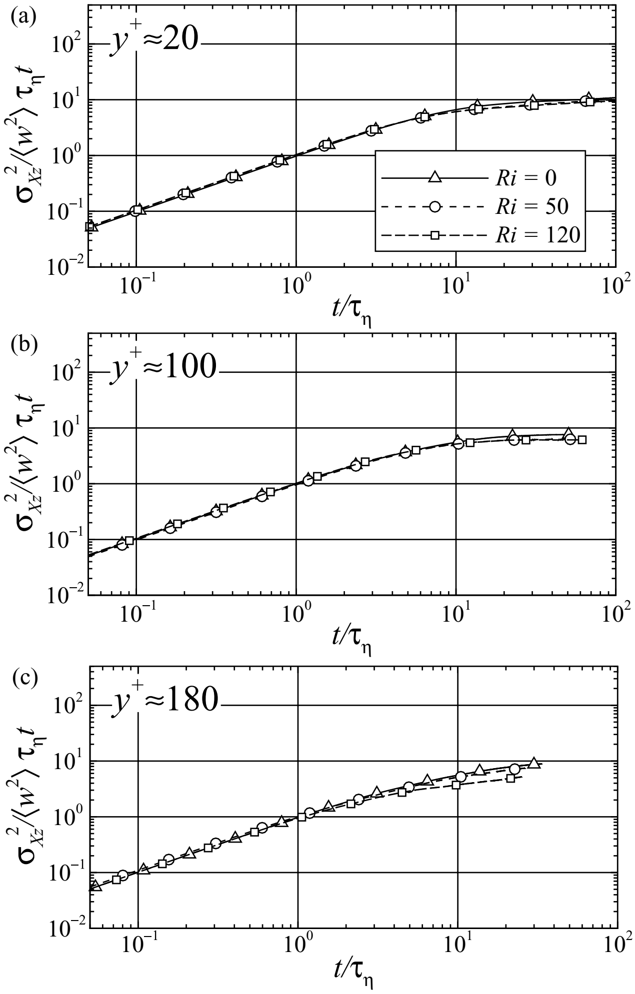

Figure 21. Mean-square dispersion of fluid particles in the spanwise direction for three different Ri_τ. The fluid particles are released at (a) the buffer layer ($y^+ \simeq 20$), (b) log-law region $y^+ \simeq 100$, and (c) channel center $y^+ \simeq 180$.

Figure 21 presents the scaled $\sigma_{X_z}^2$. In early time, the scaled dispersion in the stably stratified flows shows the same $\sim t^2$ behavior with $Ri_\tau = 0$ case. In late time, the scaled dispersion shows $\sim t$ behavior (Equation 17) except for the channel center. However, it is observed that the spanwise dispersion is slightly suppressed, and the suppression becomes larger as the distance from the wall increases, although modification is not as pronounced as in the wall-normal direction.

6.2. *The p.d.f. of particle location*

The p.d.f. for the expected wall-normal location of fluid particles are displayed in Figure 22. The p.d.f.s were calculated by using the Gaussian kernel regression after the particles migrate for $tu_\tau/\delta = 2$. About 2.5×10^4 samples were used to obtain each p.d.f. As the

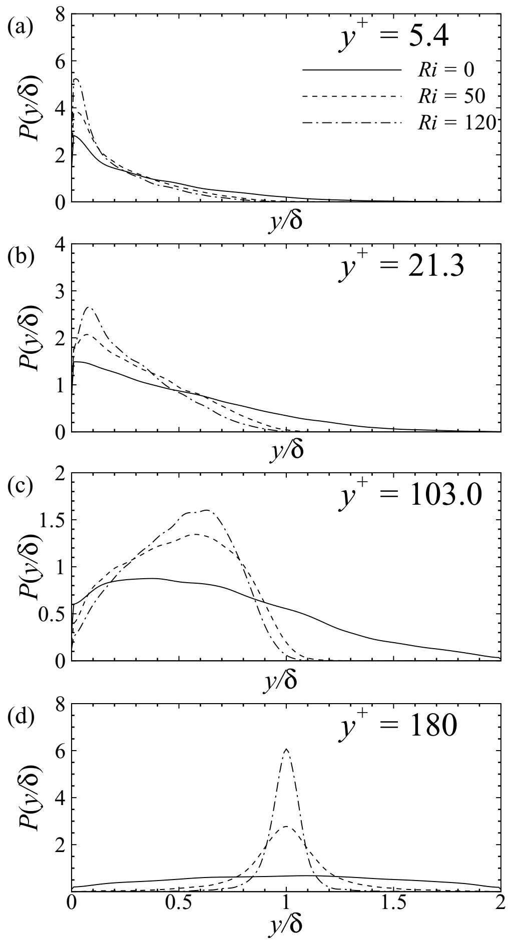

Figure 22. The p.d.f.s for the wall-normal location of fluid particles at $t_0 + 2tu_\tau/\delta$ whose initial positions are (a) in the viscous sublayer, (b) buffer layer, (c) log-law region, and (d) at the channel center.

stratification becomes stronger, the probability for fluid particles to remain near the initial release location increases dramatically. In consequence, the interaction between layers is weakened in the stably stratified channel flows [10]. It is quite astonishing to observe such a conspicuous change specially near the wall, considering that the turbulence intensities are hardly modified by the stratification.

When $Ri_\tau = 0$, the fluid particles released in the lower half [Figure 22(a–c)] are spread over the whole channel. In the stably stratified case, however, it is observed that the upward migration of fluid particles is blocked in the center region. Almost all fluid particles remain in the lower half in which they were seeded, indicating that the interaction between lower and higher halves are blocked, which is obviously caused by the internal gravity waves in the center region. This decoupling explains why the stably stratified channel flows undergo asymmetric transition between the two walls shown in previous DNS and LES results [10–12].

The p.d.f.s in the viscous sublayer show very large peaks near the release location, and the peaks are increased with increasing Ri_τ, supporting the previous finding that the viscous sublayer is loosely coupled with the rest of the flow in the strongly stratified flows [10]. Figure 23(a, d) shows some exemplary trajectories of fluid particles released in the viscous sublayer. In the neutral channel flow, most fluid particles are entrained by the streamwise vortices and are carried to the outer region. However, in the stably stratified case, fluid particles move much longer distance before being caught by the streamwise vortices. Since the ejection events are largely suppressed by buoyancy (Figure 5), the entrainment of fluid particles released in the viscous sublayer by the streamwise vortices is reduced, and this weakens the interaction between the viscous sublayer and the rest.

Figure 23(b, e) displays the trajectories of fluid particles released in the buffer layer. In a neutral flow, fluid particles exhibit large-scale oscillations induced by vortical structures, while those in stably stratified flow show relatively small rapid oscillations. As shown in Section 4, both the time and length scales of the coherent vortices are reduced under stable stratification, explaining the rapid small-scale motion. As a result, it becomes less probable for a fluid particle to move a longer distance in the vertical direction, leading to the suppression of the dispersion in the vertical direction.

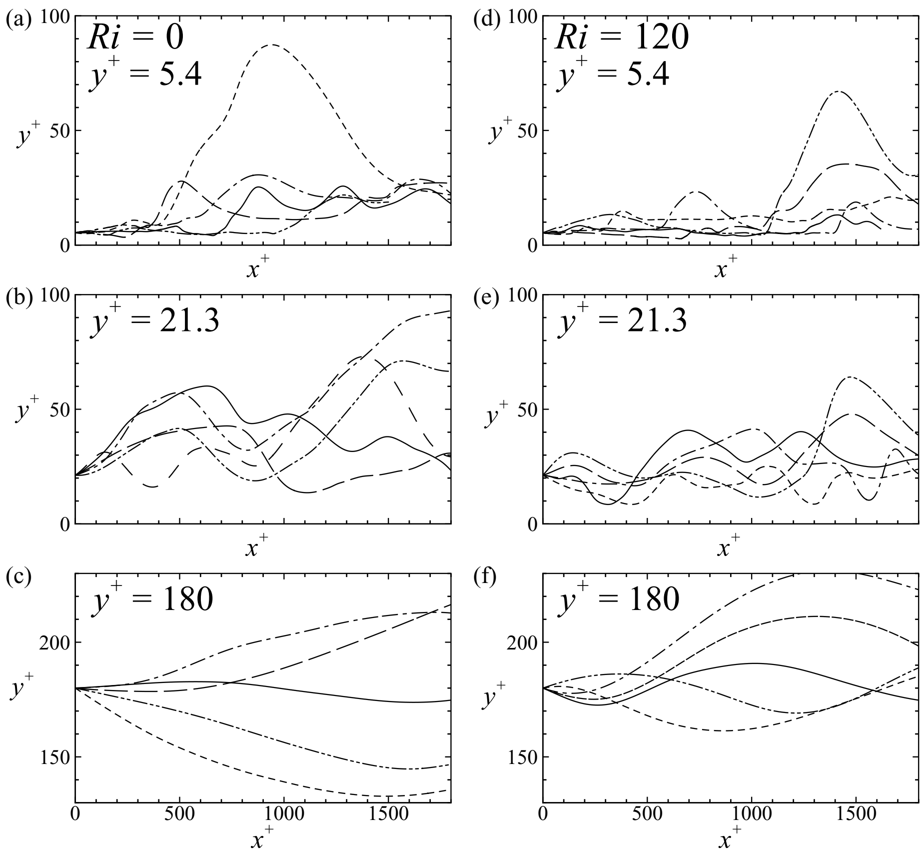

Figure 23. Sample trajectories in (a–c) neutral and (d–f) stably stratified channel flows for particles released in the (a, d) viscous sublayer, (b, e) buffer layer, and (c, f) channel center.

In Figure 22(d), it is shown that the fluid particles are trapped in the center region in stably stratified flows, while those in the neutral flow are spread through the whole channel. In Figure 23(f), it is found that the fluid-particle trajectories at the channel center show a wavelike motion in the stably stratified flows, which is obviously caused by the internal gravity waves. This oscillation of fluid particles results in the suppression of the vertical dispersion.

7. Conclusions

In this paper, we investigated the near-wall modification of the Eulerian and Lagrangian characteristics of turbulent channel flows under stable stratification by using DNSs. In the simulation, the pressure gradient was kept constant to maintain $Re_\tau = 180$, leaving the Richardson number as the only varying parameter. Turbulence statistics were obtained for the Richardson numbers ranging from 50 to 120 and were compared with the neutral case.

Although the Reynolds stress and turbulent kinetic energies in the near-wall region are not changed significantly by stratification, an investigation of the higher-order statistics, energy spectra, and quadrant analysis shows that turbulent structures connected to the Reynolds stress and kinetic energies are modified under stable stratification. The most pronounced changes come from the suppression of large-scale motions by stratification like the homogeneous turbulence. However, in channel flows, the small-scale motions become more energetic with increasing Richardson number except for the channel center region, and this leads to changes in turbulence characteristics in the near-wall region. It is shown that under strong stratification the turbulent scales in the near-wall region are decreased compared to the neutral case, making turbulence more intermittent.

It is found that the scales related with the near-wall vortical motion are also reduced by stratification. The average size of streamwise vortices becomes smaller, and the rotation speed of a fluid particle following a vortical structure becomes faster than in the neutral case. The investigation of baroclinic torque explicitly reveals the mechanism modifying turbulent structures under stable stratification. Small-size streamwise vortical structures are generated by small but nontrivial baroclinic torque acting on the streamwise vortices. It is also shown that the orientation of hairpin vortices is also changed by the spanwise baroclinic torque.

We found that the scaled mean-square dispersion in the streamwise direction remains almost unchanged, since the effect of mean streamwise velocity is much larger than that of turbulent fluctuations in the streamwise direction. The wall-normal dispersion is most seriously suppressed by stratification. Unlike the homogeneous turbulence in which only the dispersion in the direction of stratification is changed, the dispersion in the spanwise direction is suppressed in the stably stratified channel flows, implying that structural changes are involved. Some representative fluid-particle trajectories suggest that, since large-scale motions are suppressed by stratification, a fluid particle has less chance to migrate a longer distance in the vertical direction following the motion of large-scale structure in stably stratified turbulence.

The investigation of the p.d.f.s of the expected wall-normal location of fluid particles at late time reveals that since the wall-normal dispersion is largely suppressed and the interaction between layers is loosened in the stably stratified flows, the probability for a fluid particle to remain near the release location is greatly increased even at late times. It is found that almost all of the fluid particles released in the lower half of the channel could not migrate to the upper half owing to the presence of the internal gravity waves in the center region.

Acknowledgments

The authors gratefully acknowledge the supports provided by the Yonam Foundation and the Korea Science and Engineering Foundation through grant no. R01-2008-000-10664-0 and WCU Project. The authors are grateful to Dr. J. Lim for helpful discussions. Most computations were carried out in the KISTI Supercomputing Center in Korea, and their support is also gratefully acknowledged.

References

[1] E.C. Itsweire, K.N. Helland, and C.W. van Atta, *The evolution of grid-generated turbulence in stably stratified fluid*, J. Fluid Mech. 162 (1986), pp. 299–338.

[2] J.J. Rohr, E.C. Itsweire, K.N. Helland, and C.W. van Atta, *Growth and decay of turbulence in a stably-stratified shear flow*, J. Fluid Mech. 195 (1988), pp. 77–111.

[3] S.E. Holt, J.R. Koseff, and J.H. Ferziger, *A numerical study of the evolution and structure of homogeneous stably stratified sheared turbulence*, J. Fluid Mech. 237 (1992), pp. 499–539.

[4] P.J. Diamessis and K.K. Nomura, *Interaction of vorticity, rate-of-strain, and scalar gradient in stratified homogeneous sheared turbulence*, Phys. Fluids 12 (2000), pp. 1166–1188.

[5] J.J. Riley and M.-P. Lelong, *Fluid motions in the presence of strong stable stratification*, Annu. Rev. Fluid Mech. 32 (2000), pp. 613–657.

[6] O. Mètais and J.R. Herring, *Numerical simulations of freely evolving turbulence in stably stratified fluids*, J. Fluid Mech. 202 (1983), pp. 117–148.

[7] Y. Kimura and J.R. Herring, *Diffusion in stably stratified turbulence*, J. Fluid Mech. 328 (1996), pp. 252–269.

[8] S.T. Thoroddsen and C.W. van Atta, *Baroclinic generation of vorticity by an axisymmetric vortex in a linearly stratified fluid, in the passive limit*, Phys. Fluids 8 (2000), pp. 2774–2776.

[9] G.N. Coleman, J.H. Ferziger, and P.R. Spalart, P.R., *Direct numerical simulation of the stably stratified turbulent Ekman layer*, J. Fluid Mech. 244 (1992), pp. 677–712.

[10] R.P. Garg, J.H. Ferziger, S.G. Monismith, and J.R. Koseff, *Stably stratified turbulent channel flows. Part 1. Stratification regimes and turbulence suppression mechanism*, Phys. Fluids 12 (2000), pp. 2569–2594.

[11] V. Armenio and S. Sarkar, *An investigation of stably stratified turbulent channel flow using large-eddy simulation*, J. Fluid Mech. 459 (2002), pp. 1–42.

[12] O. Iida, N. Kasagi, and Y. Nagano, *Direct numerical simulation of turbulent channel flow under stable density stratification*, Int. J. Heat Mass Transfer 45 (2002), pp. 1693–1703.

[13] R. Benzi, G. Amati, C. Casciola, F. Toschi, and R. Piva, *Intermittency and scaling laws for wall bounded turbulence*, Phys. Fluids 11(6) (1999), pp. 1284–1287.

[14] F. Toschi, G. Amati, S. Succi, R. Benzi, and R. Piva, *Intermittency and structure functions in channel flow turbulence*, Phys. Rev. Lett. 82 (1999), pp. 5044–5047.

[15] C. Lee, K. Yeo, and J.-I. Choi, *Intermittent nature of acceleratoin in near-wall turbulence*, Phys. Rev. Lett. 92 (2004), art. no. 144502.

[16] J.-I. Choi, K. Yeo, and C. Lee, *Lagrangian statistics in turbulent channel flow*, Phys. Fluids 16 (2004), pp. 779–793.

[17] S.P.S. Arya, *Buoyancy effects in a horizontal flat-plate boundary layer*, J. Fluid Mech. 68 (1975), pp. 321–343.

[18] K. Fukui, M. Nakajima, and H. Ueda, *A laboratory experiment on momentum and heat transfer in the stratified surface layer*, Quart. J. R. Meteorol. Soc. 109 (1983), pp. 661–676.

[19] J. Kim, P. Moin, and R. Moser, *Turbulent statistics in fully developed channel flow at low Reynolds number*, J. Fluid Mech. 177 (1987), pp. 133–166.

[20] J. Jeong, F. Hussain, W. Schoppa, and J. Kim, *Coherent structures near the wall in a turbulent channel flow*, J. Fluid Mech. 332 (1997), pp. 185–214.

[21] S.S. Lu and W.W. Willmarth, *Measurements of the structure of the Reynolds stress in a turbulent boundary layer*, J. Fluid Mech. 60 (1973), pp. 481–511.

[22] A. La Porta, G.A. Voth, A.M. Crawford, J. Alexander, and E. *Bodenschatz, Fluid particle accelerations in fully developed turbulence*, Nature, 409 (2001), pp. 1017–1019.

[23] T. Gerz, J. Howell, and L. Mahrt, *Vortex structures and microfronts*, Phys. Fluids 6 (1994), pp. 1242–1251.

[24] K.H. Keller and C.W. van Atta, *An experimental investigation of the vertical temperature structure of homogeneous stratified shear turbulence*, J. Fluid Mech. 425 (2000), pp. 1–29.

[25] J. Jeong and F. Hussain, *On the identification of a vortex*, J. Fluid Mech. 285 (1995), pp. 69–94.
[26] F.-C. Li, Y. Kawaguchi, K. Hishida, and M. Oshima, *Investigation of turbulence structures in a drag-reduced turbulent channel flow with surfactant additive by stereoscopic particle image velocimetry*, Exp. Fluids 40 (2006), pp. 218–230.
[27] J. Zhou, R.J. Adrian, S. Balachandar, and T.M. Kendall, *Mechanisms for generating coherent packets of hairpin vortices in channel flow*, J. Fluid Mech. 387 (1999), pp. 353–396.
[28] B. Ganapathisubramani, E.K. Longmire, and I. Marusic, *Experimental investigation of vortex properties in a turbulent boundary layer*, Phys. Fluids 18 (2006), art. no. 055105-1-14.
[29] W.D. Smyth and J.N. Moum, *Length scales of turbulence in stably stratified mixing layers*, Phys. Fluids 12 (2000), pp. 1327–1342.
[30] G.T. Csanady, *Turbulent diffusion in a stratified fluid*, J. Atmos. Sci. 21 (1964), pp. 439–447.
[31] J. Weinstock, *Vertical turbulent diffusion in a stably stratified fluid*, J. Atmos. Sci. 35 (1978), pp. 1022–1027.